Wang *et al. Biochar* (2023) 5:23
https://doi.org/10.1007/s42773-023-00224-y

Biochar

ORIGINAL RESEARCH

Open Access

A theoretical study of the effect and mechanism of FeN_3-doped biochar for greenhouse gas mitigation

Hong-Rui Wang[1], Wen-Tao Zhou[1], Rui Xiong[1], Kang-Yu Zhong[1], Jing He[1], Xin Ma[2], Qing Wu[2], Pan Long[1] and Zhi-Qiang Fu[1*]

Abstract

Paddy fields are a major emission source of greenhouse gases (GHGs) [for instance, methane (CH_4), nitrous oxide (N_2O), and carbon dioxide (CO_2)] among agricultural fields. Biochar has been deemed a potential candidate for the reduction of GHGs in paddy fields. However, there is no consistent conclusion that biochar can simultaneously reduce emissions of CH_4, N_2O, and CO_2. Herein, we proposed the FeN_3-doped biochar (FG) as an excellent material for GHGs restriction in paddy fields via the first-principles calculation. The computation results indicated that the FG exhibited satisfactory adsorption ability for CH_4, CO_2, and N_2O, which improved the adsorption energies to −1.37 , −1.54, and −2.91 eV, respectively. Moreover, the density of state (DOS) analyses revealed that the factor responsible for FeN_3-doped biochar to exhibit excellent adsorption ability was the occurrence of drastic energy up- or down-shift of the electron for Fe *d*, C *p*, O *p*, or N *p* orbital upon adsorption of CH_4, CO_2, or N_2O. Our study suggested an advanced modified biochar material for reducing the GHGs emissions in paddy fields, in addition to exploring the adsorption properties and mechanisms of FeN_3-doped biochar for GHGs mitigation, which provided a strategy to explore biochar modification and efficient emission reduction materials.

Article highlights

- FeN_3-doped biochar was first proposed for GHGs mitigation in paddy fields.
- FeN_3-doped biochar exhibited excellent GHGs adsorption ability.
- FeN_3-doped biochar improved physico-chemical adsorption ability for GHGs.

Keywords Modified biochar, Fe atoms sorbent, Greenhouse gas, First-principles calculation, Adsorption mechanism

Handling Editor:Xiaoyuan Yan

*Correspondence:
Zhi-Qiang Fu
zqf_cis@hunau.edu.cn
Full list of author information is available at the end of the article

Graphical Abstract

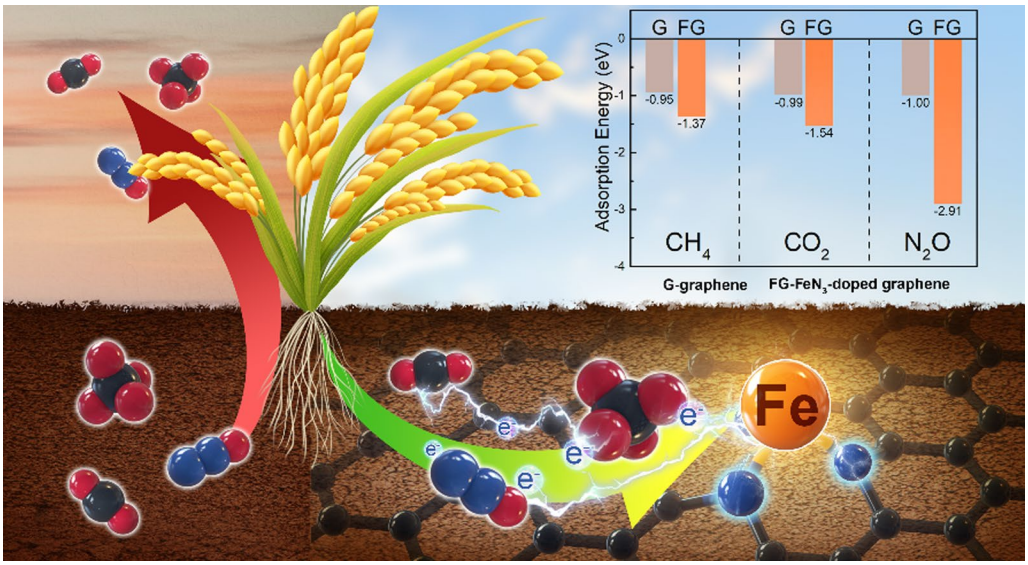

1 Introduction

Ecosystem stability and human security are facing a serious threat due to global warming (Smith and Fang 2010; Han et al. 2022). The global average temperature from 2020 to 2021 has increased by 1.1℃ compared with 1850–1900 and will continue to rise in the future (IPCC, 2021). The major inducement of global warming is the sharp enhancement of atmospheric concentrations of greenhouse gases (GHGs) [for instance, methane (CH_4), nitrous oxide (N_2O), and carbon dioxide (CO_2)] (Wang et al. 2019; Zhou et al. 2022). According to statistics in 2015, the accumulation concentrations of CH_4, N_2O, and CO_2 in the air increased by 150%, 20%, and 40%, respectively (Stocker et al. 2014; Tian et al. 2015). Paddy fields have been deemed as the primary emission source of CH_4 in agricultural fields, contributing 10% of the total CH_4 emissions (Cao et al. 2021; Shin et al. 2021). Furthermore, agricultural fields contribute approximately 66.7% of the total N_2O emissions (Akiyama et al. 2005; Van Groenigen et al. 2011; Yang and Silver 2016). Superfluous addition of nitrogen (N) fertilization and agricultural intensification increases the conversion from carbon (C) and N in soils to GHGs and their release (Wu et al. 2013; Pajares and Bohannan 2016). Multiple measures have been adopted for reducing the emission of GHGs in agricultural fields such as moisture management and the addition of amendment materials (Yan et al. 2005; Feng et al. 2013).

Biochar possesses substantial pores and abundant functional groups, which can conduce to the restriction of GHGs, and has been considered as a potential candidate for the reduction of GHGs in agricultural fields (Wu et al. 2013; Godlewska et al. 2017; Cui et al. 2021; Shakoor et al. 2021; Shin et al. 2021). The main restriction mechanisms of biochar for GHGs include: (1) biochar with abundant porosity could reduce the oxygen deficit in soils, which is helpful to retard the production of methanogens and inhibit the conversion of CH_4 (Karhu et al. 2011; Nan et al. 2021); (2) biochar can enhance the abundance of methanotrophic proteobacterial and reduce the CH_4 emission (Feng et al. 2012); (3) biochar may anchor the inorganic N in soils and avoid the conversion of inorganic N to N_2O (Cayuela et al. 2014; Dong et al. 2020); (4) biochar can lower soil acidity and control the process of nitrification and denitrification (Sohi et al. 2010; Cayuela et al. 2013); and (5) biochar is an 'electron shuttle' for electron transfer of denitrification in soils which can lead the reduction of N_2O to N_2 (Cayuela et al. 2013; Yuan et al. 2022). However, unlike for the N_2O and CO_2, researchers have different standpoints on the mitigation effect of biochar for CH_4. (Karhu et al. 2011; Wu et al. 2013; Bruun et al. 2016). For example, Jeffery et al. found that biochar could reduce the CH_4 emissions from soils (Jeffery et al. 2016), but Zhang et al. considered that biochar could improve the total CH_4 emissions from soils (Zhang et al. 2010). Thus, it is necessary to develop biochar-based modification materials for mitigating the emissions of GHGs in paddy fields. Recently, single atomic catalyst (SAC) doped carbon materials

have gathered widespread interest in the environmental field due to their low cost, excellent chemical characteristics, superior atom utilization efficiency, and abundant specific surface area (Qiao et al. 2011; Yuan and Shi 2013; Wang et al. 2015; Zhou et al. 2019). Among them, FeN_3-doped carbon materials have shown excellent performance in previous studies, which will be beneficial to improve the current issues (such as heavy metal pollution and GHG emission) in agricultural fields. For example, Gao et al. proved that FeN_3-embedded carbon possesses a good mercury adsorption ability via the first-principles calculation (Gao et al. 2019); Xie et al. found that FeN_3-doped graphene could adsorb the gas molecules (C_2H_2, H_2S, SO_2, SO_3, and O_2) (Xie et al. 2022). Thus, it is an efficient method to use the FeN_3-doped biochar as the sorbent in paddy fields which are the main emission source for GHGs. However, the adsorption effect and mechanism of FeN_3-doped biochar for mitigation of GHG emissions in paddy fields are unclear.

In this study, due to the various components in biochar, FeN_3 may possess diverse sites on biochar. Herein, according to previous studies (Okamoto 2009; Gao et al. 2019; Li et al. 2021), the first-principles calculations were carried out using graphene (G) as a simplified model to explore the inhibition effect and mechanism of G and its FeN_3-doped for GHGs. At first, the electron characteristics of G and the FeN_3-doped G (FG) were evaluated. The adsorption ability and stability between the different substrates and CH_4, N_2O, or CO_2 were then compared. Finally, the electronic properties of adsorption systems were investigated and the inhibition mechanism of CH_4, N_2O, and CO_2 adsorption on FeN_3-C were revealed. These results can provide insights that will aid in a better understanding of the effect and mechanism of SAC-doped carbon materials for GHGs mitigation in paddy fields, and the effective selection of materials for GHG mitigation.

2 Computational methodology

All the calculations were based on the first principles and carried out by the Vienna Ab Simulation Package (VASP). The exchange-correlation function has been described by the Perdew-Burke-Ernzerhof (PBE) type and the interaction between electrons and ions was considered through the projector augmented wave (PAW) method (Hohenberg and Kohn 1964; Kresse and Furthmüller 1996a, b). The construction of FG model referred to the previous study. In brief, four carbon sites were replaced by three nitrogen (N) atoms and a Fe atom site. Among them, Fe was confined in the central of three N atoms (Gao et al. 2019). The DFT-D3 was set to describe the van der Waals interaction in all the calculations for adsorption systems (Perdew et al. 1996; Zhang et al. 2020). The localized d electrons of the Fe element have been described via the DFT + U method, with the U value set to 4 eV (Zhou and Sun 2011; Wang et al. 2022a). The cutoff energy, convergence standard of energy, and force were set to 500 eV, 10^{-5} eV, and 0.02 eV $Å^{-1}$, respectively (Zhou et al. 2022). The k mesh of the structure optimization and density of state (DOS) calculations were set to $3 \times 3 \times 1$ and $11 \times 11 \times 1$ with the Gamma-centered grids (Froyen 1989; Liu et al. 2021). To avoid the interplay of the adjacent unit cells, the 15 Å vacuum layer was instituted. The formulas of adsorption energy (E_a) and differential charge density ($\Delta\rho$) are as follows:

$$E_a = E_{gas-substrate} - \left(E_{gas} + E_{substrate}\right),$$

where $E_{gas-substrate}$, E_{gas}, and $E_{substrate}$ represent the total energy after the gas molecule adsorbed on the substrate, single energy of the different gases, and different substrates, respectively (Luo et al. 2019).

$$\Delta\rho = \rho_{gas-substrate} - \rho_{gas} - \rho_{substrate},$$

where $\rho_{gas-substrate}$, $\rho_{gas,}$ and $\rho_{substrate}$ represent representhe charge density of the adsorption configuration of the gas molecule and substrate, charge density of the different gas molecules, and different substrates, respectively. The differential charge density and electron localization function (ELF) images were drawn by VESTA (Momma and Izumi 2011).

3 Results and discussion

We first studied the structural stability of the graphene substrate doped with FeN3 molecules (Fig. 1). As shown in Fig. 1a, b, the structure of FG was not planar. This phenomenon is attributed to the larger size of Fe atoms compared to the C atom, which renders Fe non-planar; further, this property may aid in providing efficient adsorption sites (Miao et al. 2021). The electronic properties of G and FG were then explained by the electron localization function (ELF) and band calculation. As the ELF plots shown, there were conspicuous electron transformations in FG, which could change the adsorption performance of G (Fig. 1c, d and Additional file 1: Fig. S1). Furthermore, band calculation was carried out to study the electron transfer ability and electronic characters. The computed results of the band showed that G and FG exhibited metallic properties and facilitated electron exchange for GHG adsorption (Fig. 1e, f).

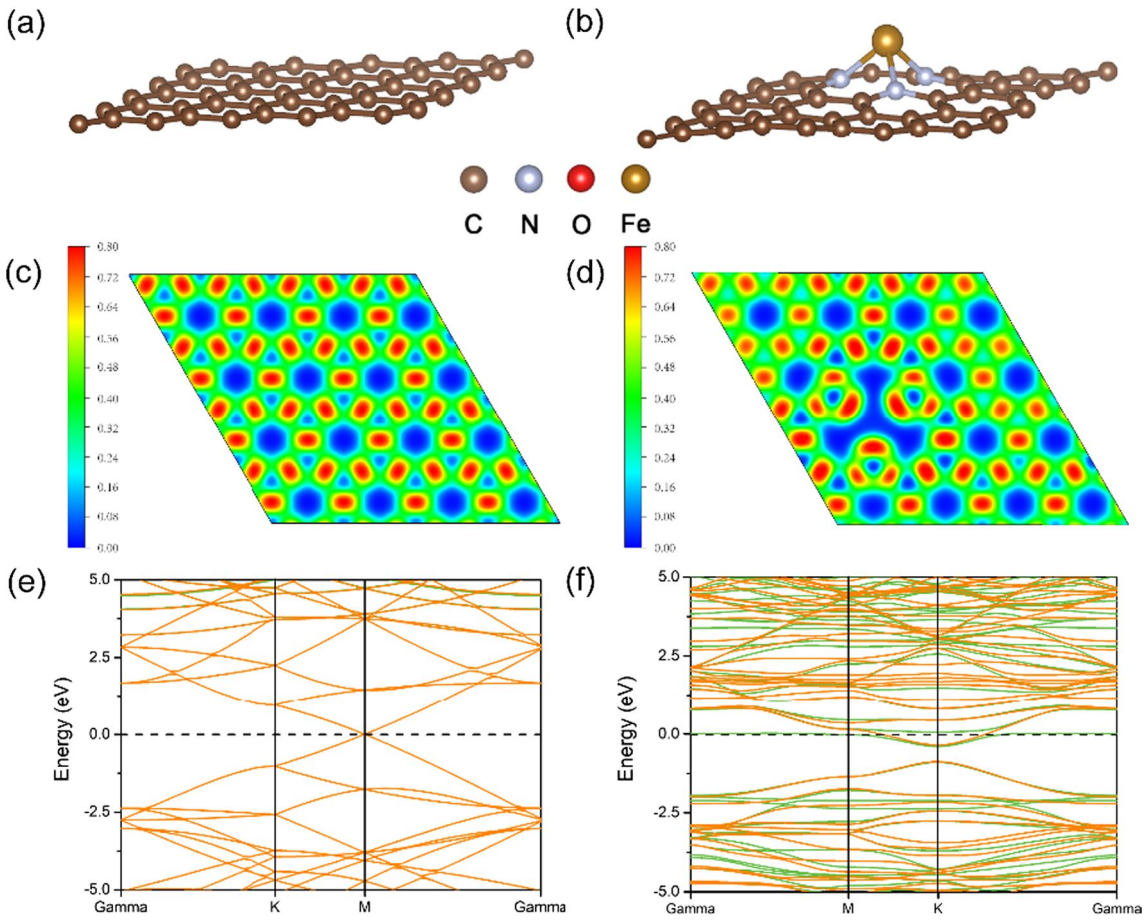

Fig. 1 Schematics of G (**a**) and FG (**b**), ELF diagrams of G (**c**) and FG (**d**), band structures of G (**e**) and FG (**f**)

Contrastingly, a distinct orbital spin in FG was observed, which is attributed to the introduction of Fe atoms, rendering can render electron transfer easy for the adsorption of GHGs (Légaré et al. 2018).

Next, the bond angle and length were used to compare the adsorption difference of G and FG for GHGs (Fig. 2a–f). Compared with the GHGs-G adsorption systems, the bond angles (H-C-H, O-C-O, N-O-N) of the GHGs-FG adsorption systems were 104.75°, 148.89°, and 99.34°, respectively, which were all lower than those of GHGs-G adsorption systems (109.26°, 179.76°, and 179.31°). These results imply the excellent anchoring ability of FG for GHGs, which can aid in reduction of GHG emissions from soil to air(Wang et al. 2022a). Besides, the CO_2 and N_2O on FG exhibit a longer bond length (1.19 Å and 1.39 Å) than those adsorbed on G (1.18 Å and 1.20 Å), which is attributed to the strong adsorption ability of FG for GHGs. However, there was no noticeable difference in bond length (1.10 Å) for CH_4 on G and FG, which may be due to the weaker electron exchangeability for FG adsorbing CH_4 than adsorbing CO_2 and N_2O. The calculations of adsorption energy were further used to analyze the anchoring performance of G and FG for GHGs. As the previous studies proposed, the small adsorption energy means the weak anchoring ability (Hou et al. 2016; Wang et al. 2022b). In contrast with the adsorption energies of CH_4, CO_2, and N_2O adsorbed on G (−0.95, −0.99, and −1.00 eV), the adsorption energies of FG for CH_4, CO_2, and N_2O all improved (−1.37, −1.54, and −2.91 eV), demonstrating the greater anchoring ability of FG for GHGs (Fig. 2g).

To comprehend the adsorption reaction mechanism, the electronic performances of the adsorption systems were computed. At the outset, the differences in the

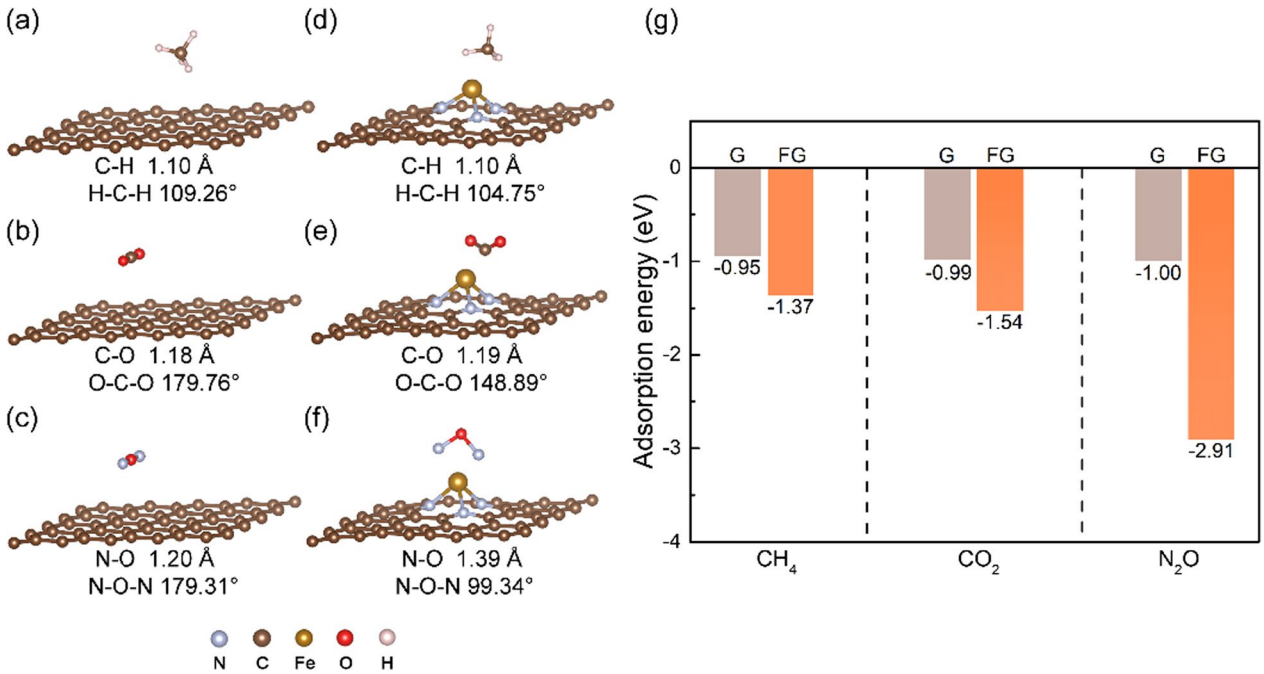

Fig. 2 Schematics of CH_4 on G (**a**) and FG (**d**), the CO_2 on G (**b**) and FG (**e**), N_2O on G (**c**) and FG (**f**), Adsorption energies of GHGs on G and FG (**g**)

electronic charge density of GHGs adsorbed on different substrates are displayed in Fig. 3 and Additional file 1: Fig. S2, to explain the status of charge transfer and redistribution. As shown in Fig. 3d–f, there were distinct existing accumulation and depletion regions of the charge in GHGs-FG adsorption systems. It is worth noting that the inferior performance of charge redistribution was observed in GHGs-G adsorption systems, despite their larger isosurface value (Fig. 3a–c). The main reason for the above differences is that the adsorption of GHGs by FG was physical chemisorption, while G only exhibited physical adsorption behavior.

The ELF plots further prove the behavior of electron charge transfer of GHGs-G or -FG adsorption systems. As shown in Fig. 4a–c, there were apparent improvements in both GHG molecules and substrates upon adsorption of GHGs on FG, with more noticeable changes displayed in neighboring atoms, especially at the direct adsorption sites. However, these performances were difficult to find in GHGs-G adsorption systems (Additional file 1: Fig. S3). The results of the electron charge density difference and ELF plots proved that the distribution of the charges changed while the GHGs adsorbed on FG. The Bader charge analysis was computed to further evaluate the charge transfer ability of GHGs-G or -FG adsorption systems. As the previous study confirmed, the greater the charge transformation, the stronger the ability of molecule restriction (Wang et al. 2022b). Combined with the low electron transfer numbers of G for CH_4, CO_2, and N_2O (0.00, 0.01, and 0.02 e), the FG showed satisfactory results for GHG adsorption, wherein the number of electron transfers for CH_4, CO_2, and N_2O increased to 0.03, 0.42, and 0.83 e, respectively. Additionally, as shown in Additional file 1: Table S1, the number of electron changes mainly occurred in Fe atoms and GHG molecules, with a small difference in the number of electron changes in C atoms, which is consistent with the implications of Figs. 3 and 4.

The density of state (DOS) and partial density of state (PDOS) analyses were further used for an in-depth evaluation of the mechanism of electron transfer and orbital contribution for adsorption systems. As shown in Fig. 5a–c, the energy shift could be seen after CH_4, CO_2, or N_2O was adsorbed on FG. These results illustrate that the electron state has been transformed in GHGs-FG adsorption systems and prove that the FG can inhibit GHGs via physico-chemical adsorption. However, there is no evidence that the energy shift occurred during the CH_4, CO_2, or N_2O adsorbing on G, implying the presence of only physical adsorption behavior in GHGs-G

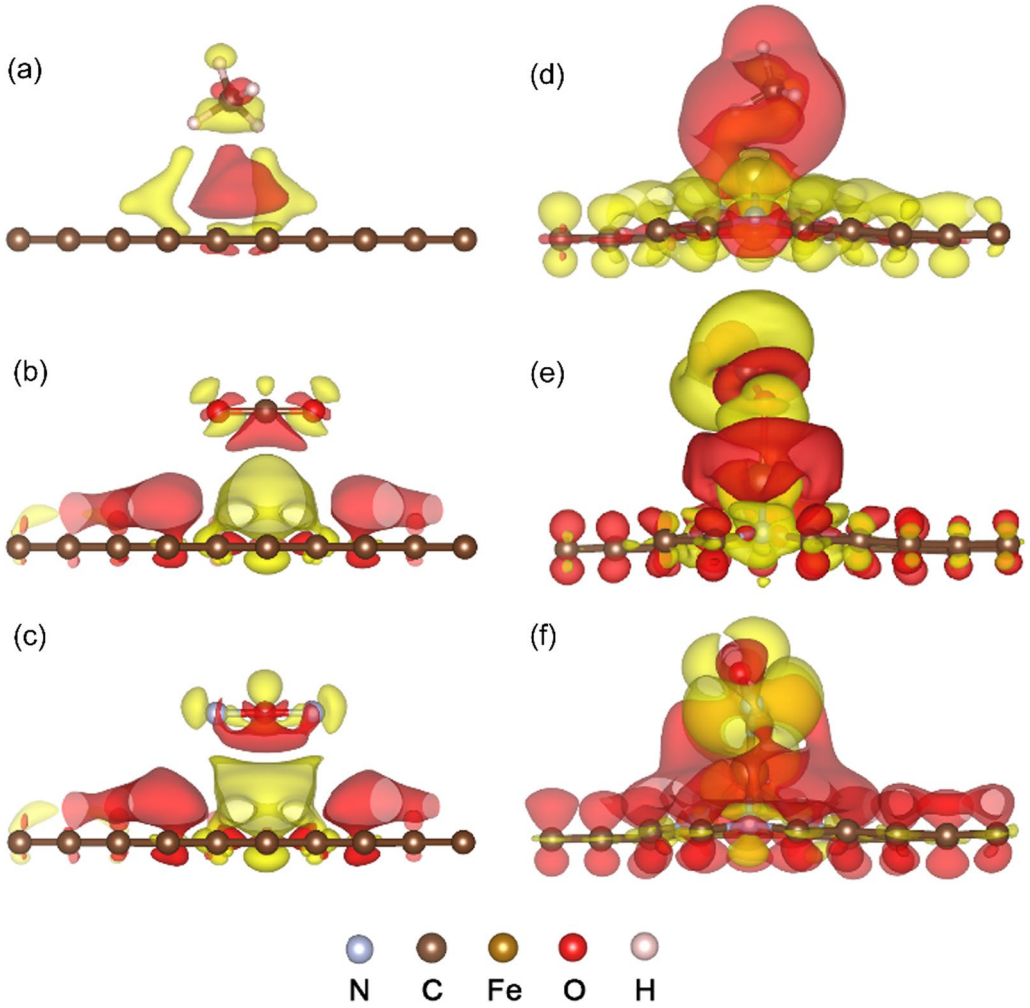

Fig. 3 Charge density difference of the front views of CH_4 on G (**a**) and FG (**d**), CO_2 on G (**b**) and FG (**e**), N_2O on G (**c**) and FG (**f**) The isosurface is set to 6×10^{-5} e Å^{-3} in GHGs-G and set to 4×10^{-4} e Å^{-3} in GHGs-FG. Note that red and yellow correspond to charge depletion and charge accumulation

adsorption systems. In addition, the PDOS analyses of GHGs-FG were used to study the orbital contribution. As shown in Fig. 5d–f and Additional file 1: Fig. S4, there was a clear exhibition that a drastic energy up- or down-shift of the electron of FG (Fe *d* and N *p* orbital) and GHGs (C *p*, O *p*, and N *p* orbital) occured when CH_4, CO_2, or N_2O adsorbed on FG, which may be the major induction for the electron energy shift in GHGs-FG adsorption systems. However, there was no noticeable electron energy shift electron in GHGs-G adsorption systems, which provided evidence that G could restrict CH_4, CO_2, or N_2O by physical adsorption alone (Additional file 1: Fig. S5).

4 Conclusions

In summary, we have proposed an effectively modified biochar material, FeN_3-doped biochar, to reduce the emissions of GHGs in paddy fields and revealed the adsorption effect and mechanism via first principles calculations. Comparing with pure biochar, the FeN_3-doped biochar exhibited satisfactory adsorption ability for various GHGs in paddy fields (CH_4, CO_2, and N_2O), which not only changed the structure of GHG molecules, but also improved the adsorption energies to −1.37, −1.54, and −2.91 eV, respectively. The electron charge density

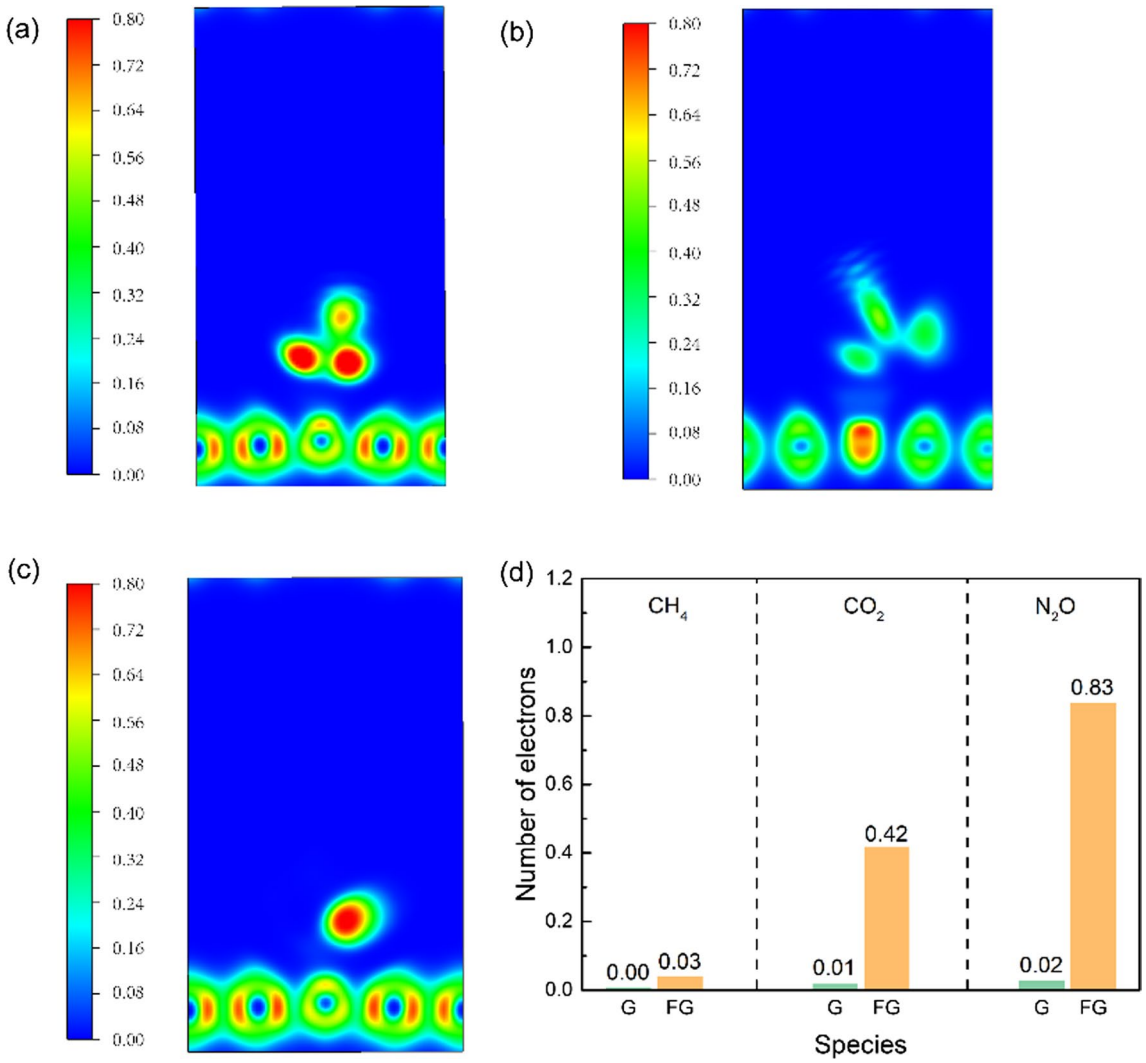

Fig. 4 ELF diagrams of CH_4 (**a**), CO_2 (**b**) and N_2O (**c**) on FG. **d** The number of charge transfer of the GHGs on G and FG

difference, ELF, and Bader charge analyses further confirmed that the FeN_3-doped biochar displayed physicochemical adsorption ability, which was different from that of pure biochar. In addition, the DOS and PDOS analyses revealed that the factor responsible for FeN_3-doped biochar to exhibit excellent adsorption ability is occurrence of the drastic energy up- or down-shift of the electron for Fe *d*, C *p*, O *p*, or N *p* orbitals upon adsorption of CH_4, CO_2, or N_2O.

Consequently, our study suggested an advanced modified biochar material for reducing the GHG emissions in paddy fields and investigated the adsorption property and mechanism of FeN_3-doped biochar for GHG mitigations, which provided a strategy for the exploration of biochar modification and efficient emission reduction materials.

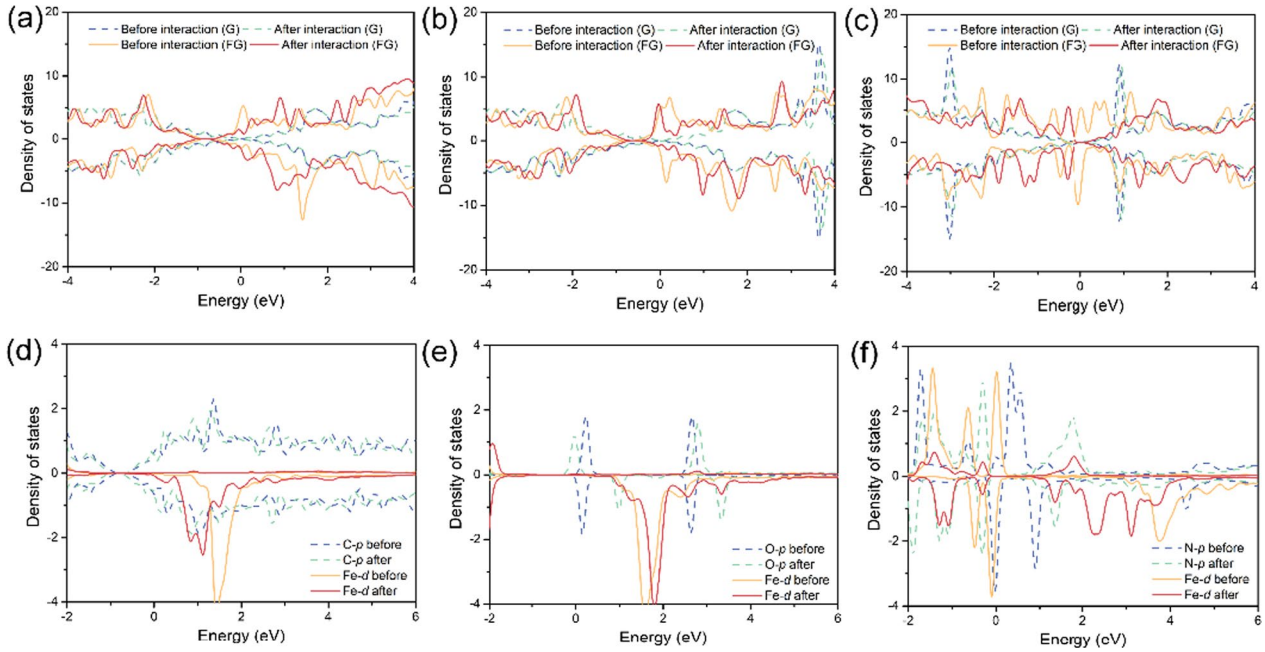

Fig. 5 The density of states of CH_4 (**a**), CO_2 (**b**) and N_2O (**c**) on G and FG. The partial density of states of CH_4 (**d**), CO_2 (**e**) and N_2O (**f**) on FG

Supplementary Information

The online version contains supplementary material available at https://doi.org/10.1007/s42773-023-00224-y.

Additional file 1: Fig. S1 ELF diagram of thetop view of Fe@G. **Fig.S2** Charge density difference of the top views ofCH_4 on G (**a**) and FG (**d**), the CO_2 on G (**b**) and FG (**e**), the N_2O on G (**c**)and FG (**f**), The isosurface is set to6×10^{-5} e $Å^{-3}$ in GHGs-G and set to 4×10^{-4} e $Å^{-3}$in GHGs-FG. Note that red and yellow correspond to charge depletion and chargeaccumulation. **Fig.S3** ELF diagram of CH_4 (**a**), CO_2 (**b**) and N_2O (**c**) on G. **Fig. S4** The partial density of states of N *p* orbital of CH_4 (**d**), CO_2 (**e**) and N_2O(**f**) on FG. **Fig. S5** The partial density of states of CH_4(**d**), CO_2 (**e**) and N_2O(**f**) on G. **Table S1.** The number of charge transfers of the GHGs on FG.

Acknowledgements

This work was carried out in part using hardware and/or software provided by the High Performance Computing Center of Central South University.

Author contributions

Z-QF: Conception and design of the study, approval of the version of the manuscript to be published; H-RW performed the study, analyzed the data; H-RW and JH wrote the manuscript; W-TZ, RX, XM and QW provided guidance on the data analysis; K-YZ and PL revised the manuscript critically for important intellectual content. All authors read and approved the final manuscript.

Funding

This work was supported by National Key Research and Development Programs (2022YFD2300305), the Natural Science Foundation of Hunan Province (2021JJ30319), Graduate Research Innovation Project of Hunan Agricultural University.

Availability of data and materials

All data generated or analysed during this study are included in this article.

Declarations

Competing interests

The author declare that they have no known competing financial interests or personal relationships that could have appeared to influence the work reported in this paper.

Author details

[1]College of Agronomy, Hunan Agricultural University, Changsha 410128, People's Republic of China. [2]College of Chemistry and Chemical Engineering, Information and Network Center, Central South University, Changsha 410083, China.

Received: 17 November 2022 Revised: 1 April 2023 Accepted: 4 April 2023
Published online: 18 April 2023

References

Akiyama H, Yagi K, Yan X (2005) Direct N2O emissions from rice paddy fields: summary of available data. Glob Biogeochem Cycle. https://doi.org/10.1029/2004GB002378

Bruun E, Cross A, Hammond J, Nelissen V, Rasse DP, Hauggaard-Nielsen H (2016) Biochar carbon stability and effect on greenhouse gas emissions. Biochar in European soils and agriculture. Routledge, pp 187–205. 10.4324/9781315884462-16/

Cao Y, Shan Y, Wu P, Zhang P, Zhang Z, Zhao F, Zhu T (2021) Mitigating the global warming potential of rice paddy fields by straw and straw-derived biochar amendments. Geoderma 396:115081. https://doi.org/10.1016/j.geoderma.2021.115081

Cayuela ML, Sánchez-Monedero MA, Roig A, Hanley K, Enders A, Lehmann J (2013) Biochar and denitrification in soils: when, how much and why does biochar reduce N_2O emissions? Sci Rep 3:1–7. https://doi.org/10.1038/srep01732

Cayuela ML, Van Zwieten L, Singh BP, Jeffery S, Roig A, Sánchez-Monedero MA (2014) Biochar's role in mitigating soil nitrous oxide emissions: a review and meta-analysis. Agric Ecosyst Environ 191:5–16. https://doi.org/10.1016/j.agee.2013.10.009

Cui J, Glatzel S, Bruckman VJ, Wang B, Lai DYF (2021) Long-term effects of biochar application on greenhouse gas production and microbial community in temperate forest soils under increasing temperature. Sci Total Environ 767:145021. https://doi.org/10.1016/j.scitotenv.2021.145021

Dong W, Walkiewicz A, Bieganowski A, Oenema O, Nosalewicz M, He C, Zhang Y, Hu C (2020) Biochar promotes the reduction of N_2O to N_2 and concurrently suppresses the production of N_2O in calcareous soil. Geoderma 362:114091. https://doi.org/10.1016/j.geoderma.2019.114091

Feng Y, Xu Y, Yu Y, Xie Z, Lin X (2012) Mechanisms of biochar decreasing methane emission from chinese paddy soils. Soil Biol Biochem 46:80–88. https://doi.org/10.1016/j.soilbio.2011.11.016

Feng J, Chen C, Zhang Y, Song Z, Deng A, Zheng C, Zhang W (2013) Impacts of cropping practices on yield-scaled greenhouse gas emissions from rice fields in China: a meta-analysis. Agric Ecosyst Environ 164:220–228. https://doi.org/10.1016/j.agee.2012.10.009

Froyen S (1989) Brillouin-zone integration by Fourier quadrature: special points for superlattice and supercell calculations. Phys Rev B 39:3168. https://doi.org/10.1103/PhysRevB.39.3168

Gao X, Zhou Y, Liu S, Tan Y, Cheng Z, Shen Z (2019) FeN_3-embedded carbon as an efficient sorbent for mercury adsorption: a theoretical study. Chem Eng J 374:1337–1343. https://doi.org/10.1016/j.cej.2019.04.189

Godlewska P, Schmidt HP, Ok YS, Oleszczuk P (2017) Biochar for composting improvement and contaminants reduction. A review. Bioresour Technol 246:193–202. https://doi.org/10.1016/j.biortech.2017.07.095

Han L, Chen L, Li D, Ji Y, Feng Y, Feng Y, Yang Z (2022) Influence of polyethylene terephthalate microplastic and biochar co-existence on paddy soil bacterial community structure and greenhouse gas emission. Environ Pollut 292:118386. https://doi.org/10.1016/j.envpol.2021.118386

Hohenberg P, Kohn W (1964) Inhomogeneous Electron Gas. Phys Rev 136:B864. https://doi.org/10.1103/PhysRev.136.B864

Hou TZ, Chen X, Peng HJ, Huang JQ, Li BQ, Zhang Q, Li B (2016) Design principles for heteroatom-doped nanocarbon to achieve strong anchoring of polysulfides for lithium-sulfur batteries. Small 12:3283–3291. https://doi.org/10.1002/smll.201600809

IPCC (2021) Climate change 2021: the physical science. Basis contribution of working group I to the sixth assessment report of the intergovernmental panel on climate change. IPCC, Cambridge

Jeffery S, Verheijen FGA, Kammann C, Abalos D (2016) Biochar effects on methane emissions from soils: a meta-analysis. Soil Biol and Biochem 101:251–258. https://doi.org/10.1016/j.soilbio.2016.07.021

Karhu K, Mattila T, Bergström I, Regina K (2011) Biochar addition to agricultural soil increased CH_4 uptake and water holding capacity-results from a short-term pilot field study. Agric Ecosyst Environ 140:309–313. https://doi.org/10.1016/j.agee.2010.12.005

Kresse G, Furthmüller J (1996a) Efficiency of ab-initio total energy calculations for metals and semiconductors using a plane-wave basis set. Comput Mater Sci 6:15–50. https://doi.org/10.1016/0927-0256(96)00008-0

Kresse G, Furthmüller J (1996b) Efficient iterative schemes for ab Initio Total-Energy Calculations using a Plane-Wave basis set. Phys Rev B 54:11169. https://doi.org/10.1103/PhysRevB.54.11169

Légaré M-A, Bélanger-Chabot G, Dewhurst RD, Welz E, Krummenacher I, Engels B, Braunschweig H (2018) Nitrogen fixation and reduction at boron. Science 359:896–900. https://doi.org/10.1126/science.aaq1684

Li B, Shao Z-G, Feng Y-T (2021) First-principles investigation of CO and CO_2 adsorption on pristine and Fe-doped planar carbon allotrope net-Y. Phys Chem Chem Phys 23:12771–12779

Liu Z, Huang T, Chang H, Wang F, Wen J, Sun H, Hossain M, Xie Q, Zhao Y, Wu Y (2021) Computational design of single Mo Atom Anchored defective Boron Phosphide monolayer as a high-performance Electrocatalyst for the Nitrogen reduction reaction. Energy Environ Mater 4:255–262. https://doi.org/10.1002/eem2.12120

Luo J, Sun M, Ritt CL, Liu X, Pei Y, Crittenden JC, Elimelech M (2019) Tuning pb(II) adsorption from aqueous solutions on ultrathin Iron oxychloride (FeOCl) nanosheets. Environ Sci Technol 53:2075–2085. https://doi.org/10.1021/acs.est.8b07027

Miao W, Liu Y, Wang D, Du N, Ye Z, Hou Y, Mao S, Ostrikov KK (2021) The role of Fe-Nx single-atom catalytic sites in peroxymonosulfate activation: formation of surface-activated complex and non-radical pathways. Chem Eng J 423:130250. https://doi.org/10.1016/j.cej.2021.130250

Momma K, Izumi F (2011) VESTA 3 for three-dimensional visualization of crystal, volumetric and morphology data. J Appl Cryst 44:1272–1276. https://doi.org/10.1107/S0021889811038970

Nan Q, Xin L, Qin Y, Waqas M, Wu W (2021) Exploring long-term effects of biochar on mitigating methane emissions from paddy soil: a review. Biochar 3:125–134. https://doi.org/10.1007/s42773-021-00096-0

Okamoto Y (2009) First-principles molecular dynamics simulation of O_2 reduction on nitrogen-doped carbon. Appl Surf Sci 256:335–341

Pajares S, Bohannan BJM (2016) Ecology of nitrogen fixing, nitrifying, and denitrifying microorganisms in tropical forest soils. Front Microbiol 7:1045. https://doi.org/10.3389/fmicb.2016.01045

Perdew JP, Burke K, Ernzerhof M (1996) Generalized gradient approximation made simple. Phys Rev Lett 77:3865. https://doi.org/10.1103/PhysRevLett.77.3865

Qiao B, Wang A, Yang X, Allard LF, Jiang Z, Cui Y, Liu J, Li J, Zhang T (2011) Single-atom catalysis of CO oxidation using Pt_1/FeO_x. Nat Chem 3:634–641. https://doi.org/10.1038/nchem.1095

Shakoor A, Shahzad SM, Chatterjee N, Arif MS, Farooq TH, Altaf MM, Tufail MA, Dar AA, Mehmood T (2021) Nitrous oxide emission from agricultural soils: application of animal manure or biochar? A global meta-analysis. J Environ Manage 285:112170. https://doi.org/10.1016/j.jenvman.2021.112170

Shin J, Park D, Hong S, Jeong C, Kim H, Chung W (2021) Influence of activated biochar pellet fertilizer application on greenhouse gas emissions and carbon sequestration in rice (Oryza sativa L.) production. Environ Pollut 285:117457. https://doi.org/10.1016/j.envpol.2021.117457

Smith P, Fang C (2010) A warm response by soils. Nature 464:499–500. https://doi.org/10.1038/464499a

Sohi SP, Krull E, Lopez-Capel E, Bol R (2010) Chap. 2-A review of biochar and its use and function in soil. Adv Agron 105:47–82. https://doi.org/10.1016/S0065-2113(10)05002-9

Stocker T, Plattner G-K, Dahe Q (2014) IPCC climate change 2013: the physical science basis-findings and lessons learned. Egu General Assembly Conference

Tian H, Chen G, Lu C, Xu X, Hayes DJ, Ren W, Pan S, Huntzinger DN, Wofsy SC (2015) North american terrestrial CO_2 uptake largely offset by CH_4 and N_2O emissions: toward a full accounting of the greenhouse gas budget. Clim Change 129:413–426. https://doi.org/10.1007/s10584-014-1072-9

Van Groenigen KJ, Osenberg CW, Hungate BA (2011) Increased soil emissions of potent greenhouse gases under increased atmospheric CO_2. Nature 475:214–216. https://doi.org/10.1038/nature10176

Wang Y-G, Mei D, Glezakou V-A, Li J, Rousseau R (2015) Dynamic formation of single-atom catalytic active sites on ceria-supported gold nanoparticles. Nat Commun 6:1–8. https://doi.org/10.1038/ncomms7511

Wang S, Ma S, Shan J, Xia Y, Lin J, Yan X (2019) A 2-year study on the effect of biochar on methane and nitrous oxide emissions in an intensive rice-wheat cropping system. Biochar 1:177–186. https://doi.org/10.1007/s42773-019-00011-8

Wang H, Hu J, Zhou W, Long P, Ma X, Zhang F, Wu Y, Wu X, Dai J, Fu Z (2022a) Capture mechanism of Cadmium in Agricultural Soil Via Iron-Modified Graphene. Inorganics 10:150. https://doi.org/10.3390/inorganics10100150

Wang H, Lai K, Guo F, Long B, Zeng X, Fu Z, Wu X, Xiao Y, Dou S, Dai J (2022b) Theoretical calculation guided materials design and capture mechanism for Zn-Se batteries via heteroatom-doped carbon. Carbon Neutral 1:59–67. https://doi.org/10.1002/cnl2.5

Wu F, Jia Z, Wang S, Chang SX, Startsev A (2013) Contrasting effects of wheat straw and its biochar on greenhouse gas emissions and enzyme activities in a chernozemic soil. Biol Fertil Soils 49:555–565. https://doi.org/10.1007/s00374-012-0745-7

Xie T, Wang P, Tian C, Zhao G, Jia J, He C, Zhao C, Wu H, Michel C (2022) The investigation of adsorption behavior of gas molecules on FeN3-doped graphene. J Sens. https://doi.org/10.1155/2022/9306741

Yan X, Yagi K, Akiyama H, Akimoto H (2005) Statistical analysis of the major variables controlling methane emission from rice fields. Glob Change Biol 11:1131–1141. https://doi.org/10.1111/j.1365-2486.2005.00976.x

Yang WH, Silver WL (2016) Net soil-atmosphere fluxes mask patterns in gross production and consumption of nitrous oxide and methane in a managed ecosystem. Biogeosciences 13:1705–1715. https://doi.org/10.5194/bg-13-1705-2016

Yuan W, Shi G (2013) Graphene-based gas sensors. J Mater Chem A 1:10078–10091. https://doi.org/10.1039/C3TA11774J

Yuan D, Wang G, Hu C, Zhou S, Clough TJ, Wrage-Mönnig N, Luo J, Qin S (2022) Electron shuttle potential of biochar promotes dissimilatory nitrate reduction to ammonium in paddy soil. Soil Biol Biochem 172:108760. https://doi.org/10.1016/j.soilbio.2022.108760

Zhang A, Cui L, Pan G, Li L, Hussain Q, Zhang X, Zheng J, Crowley D (2010) Effect of biochar amendment on yield and methane and nitrous oxide emissions from a rice paddy from Tai Lake plain, China. Agric Ecosyst Environ 139:469–475. https://doi.org/10.1016/j.agee.2010.09.003

Zhang F, Guo X, Xiong P, Zhang J, Song J, Yan K, Gao X, Liu H, Wang G (2020) Interface Engineering of MXene Composite Separator for High-Performance Li-Se and Na-Se Batteries. Adv Energy Mater 10:2000446. https://doi.org/10.1002/aenm.202000446

Zhou J, Sun Q (2011) Magnetism of phthalocyanine-based organometallic single porous sheet. J Am Chem Soc 133:15113–15119. https://doi.org/10.1021/ja204990j

Zhou Y, Gao G, Kang J, Chu W, Wang L-W (2019) Transition metal-embedded two-dimensional C_3N as a highly active electrocatalyst for oxygen evolution and reduction reactions. J Mater Chem A 7:12050–12059. https://doi.org/10.1039/C9TA01389J

Zhou W, Zhang Y, Zhong K, Xiong R, Long P, Xu Y, Ma X, Wu Q, Wang H, Fu Z (2022) Ferrate-modified Biochar for Greenhouse Gas Mitigation: first-principles calculation and Paddy Field trails. Agronomy 12:2661. https://doi.org/10.3390/agronomy12112661